Int J Adv Manuf Technol (2013) 68:175–186
DOI 10.1007/s00170-012-4717-8

ORIGINAL ARTICLE

Effects of tool diameters on the residual stress and distortion induced by milling of thin-walled part

Xiaohui Jiang · Beizhi Li · Jianguo Yang · Xiao Yan Zuo

Received: 15 August 2012 / Accepted: 27 December 2012 / Published online: 16 January 2013

Abstract Residual stress has a sustained impact on the deformation of thin-walled parts after processing, raising the strict restrictions required in their using procedure. In general, with regard to thin-walled parts, different processing parameters will affect the distortion and residual stress generation of the workpiece, which play the key role in the machining. However, controlling the material removal rate is also quite critical to machining of thin-walled parts. In order to reach these goals, based on the relation between residual stress and uncut chip thickness (UCT), a method is proposed by optimizing the milling tool diameters. The research finding reveals that, by improving the tool diameter, at the same circular position, smaller UCT can be achieved. In addition, take 6 and 12 mm tool diameter as analysis cases; larger tool diameter can reduce the residual tensile stress distribution significantly (the ratio ranges from 13.9 to 34.7 %) and improve the material removal rate. Moreover, a typical thin-walled part is evaluated using different tool diameters (6 and 12 mm) by experiments, as the final distortion can be decreased by 60 % with 12-mm tool diameter. The distribution of machined surface and subsurface residual stress is turning to be more uniform. Hence, it proves that, under the goals of maintaining machining accuracy and material removal rate, also improving the distribution of residual stress, it is possible to achieve by controlling the UCT (tool diameters) in the processing of thin-walled. All these findings can help to enhance the milling precision of thin-walled parts, as well as control and optimize the residual stress distribution.

X. Jiang · B. Li (✉) · J. Yang · X. Y. Zuo
College of Mechanical Engineering, Donghua University, Shanghai, China
e-mail: lbzhi@dhu.edu.cn

Keywords Residual stress · Distortion · Tool diameters · Milling

1 Introduction

As the growing development of aerospace field, the requirements of the processing quality of aluminum alloy thin-walled parts are increasing. Especially in order to meet the machining accuracy, as well as decrease the machined surface and subsurface residual stress, many efforts have been put on these. However, during the machining process of the complex thin-walled parts, the factors such as cutting force, heat, and clamping forces are difficult to control, which make it is not easy to optimize residual stress. Typically, mechanical stress, thermal stress, and coupled effects of phase transformation stress will determine the final formation of residual stress; based on these factors, how to control and optimize these sources are the key points for the researchers and engineers in different areas. In order to analyze and control the residual stress, finite element methods [1–4], numerical methods [5–8], and experimental methods [9–12] are used to predict and evaluate the residual stress distribution. All these studies show that through effective combinations of finite element methods, numerical method, and experimental verification, such as Jacobus et al. [13], Wei and Wang [14], and Outeiroa et al. [15], providing well references for exploring the distribution of residual stress generation law and improving the processing accuracy of thin-walled parts.

With the help of the several methods discussed above, many scholars optimized the generation of residual stress by analyzing different processing parameters. For instance, Kuang and Wu [16] found that the cutting speed, feed rate, etc. played major impact on the residual stress generation, while the major impact was the thermal loading. Mohammadpour et al. [17]

presented that the maximum residual tensile stress increased as the cutting linear speed and the feed rates improved. Fan et al. [18] investigated the influence of tool angles (rake and relief angles) on the residual stress distribution. They reported that different tool rake angles would affect the residual stress, and the residual tensile stress gradually became larger as the angles increase from −15° to 0°, while smaller from 0° to 15°. In addition, Mohamed et al. [19] observed that the rounded corners of the tool edges would increase the residual tensile stress of the workpiece surface and also increase the internal depth of maximum compressive residual stress, but did not affect the surface residual tensile stress. Tang et al. [20] and Lin et al. [21] noted that the larger tooth wear of tool side would increase the magnitude of the residual tensile stress of the machined surface and subsurface, as well as the internal depth of maximum compressive residual stress. Muñoz-Sánchez et al. [22] had similar conclusions in their research. Zong et al. [3] concluded that the shape of the workpiece affected the residual stress generation. Robinson et al. [23] discussed the effects of material sensitivity of the quenching process for different aluminum alloys (7010 and 7050); as the initial residual stress generation, the less sensitive material (7010) would generate larger residual tensile stress, which provided a reference for the material selection of thin-walled parts. Recently, Richter-Trummer et al. [24] studied the influence of clamping force of friction stir welding on the residual stress and distortion; the results gave a meaningful information on clamping force setup.

These studies have laid the basis for understanding residual stress generation processing and, at a certain level, improved the subsequent optimization on controlling residual stress. However, there are no discussions concerning on the material removal rate and based on this factor to analyze the residual stress generation. Though using high cutting linear speed, the material removal rate can improve greatly, higher residual tensile stress will be produced [25]. In this case, related discussions and research are conducted in this paper in order to guarantee the machining curacy and production efficiency. In the previous study [26], it is found that uncut chip thickness (UCT) has the direct relation with residual stress. While for the same feed rate, tool diameter is another factor which will affect the UCT. Hence, with the goal of improving the material removal rate, the tool diameters are taken as the optimized target. A simplified thin-walled part is selected in the experimental and finite element (FE) simulations, which is conducted to analyze the cutting forces, temperature, residual stresses (surface and subsurface), and distortion. It is noted that, by increasing the tool diameter, the residual stress and distortion can be decreased and controlled accordingly, as well as the material removal rate is increased.

Table 2 Main mechanical properties of 7050-T7451

Yield stress (MPa)	Tensile stress (MPa)	Young's modulus (GPa)	Density (kg/m^3)	Poisson's ratio
443	512	72.2	2830	0.33

2 Simulation procedures

2.1 Machining simulation

No matter whether mechanical cutting or cold forming, the material flow stress plays a decisive role in the formation of mechanical, temperature, and residual stress. Therefore, in the simulation analysis, the most critical part is inputting the accurate flow stress data of used material. In this paper, the material Al7050-T7451 is utilized. The flow stress curve is described in [27], its chemical composition is shown in Table 1 [28], and the main mechanical properties is presented in Table 2. For predicting the cutting forces and temperature using FE simulations [3, 29], there are plenty of material models compared in [30]; each model has its own advantages and disadvantages. In this paper, the model of power law is presented in Eq.1, and detailed material model parameters can be found in [31].

$$\sigma\left(\varepsilon^p, \dot{\varepsilon}, T\right) = g(\varepsilon^p) \cdot \Gamma\left(\dot{\varepsilon}\right) \cdot \Theta(T) \tag{1}$$

where $g(\varepsilon^p)$ is strain hardening, $\Gamma\left(\dot{\varepsilon}\right)$ is strain rate sensitivity, and $\Theta(T)$ is thermal softening.

As the summary in the introduction part, numerical methods and finite element methods can be used to predict residual stress. In this paper, combined with existing equipment and software conditions, AdvantEdge^{TM} is selected to simulate the processing of high-speed milling. Triangular elements of tool and workpiece are utilized in the simulation, and the maximum and minimum mesh sizes of element are 0.03 and 0.16 mm, respectively. The simulation model is presented in Fig. 1, and the other

Table 1 7050-T7451 chemical composition (in percentage)

Al	Co	Cr	Fe	Mg	Mn	Si	Ti	Zn	Zr
88.305	2.3	0.4	0.15	2.25	0.1	0.12	0.06	6.2	0.115

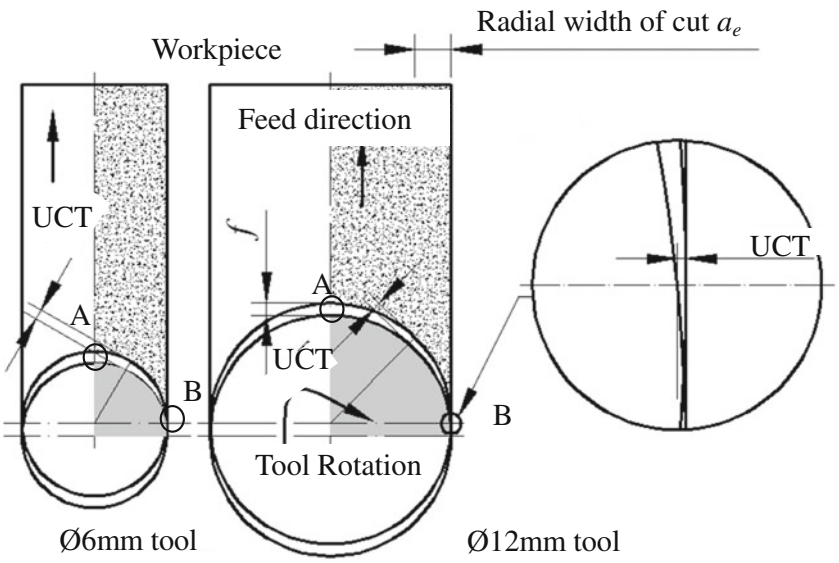

Fig. 1 UCT analysis under different tool diameters

relevant processing parameters are shown in Table 3. This software is good at predicting the cutting force, temperature, and residual stress, such as in [32, 33]. The advantages can be summarized as follows: (1) in the preprocessing, the adaptive meshing sizes can be set up, which can effectively improve the predictive ability of the stress and strain and ultimately improve the prediction accuracy of residual stress. (2) In the self-calculation model of residual stress defined in the preprocessing, after the cutting processing is completed, the mechanical and thermal loading of the workpiece material is released to calculate the residual stress, which makes it easy to operate and enhance the accuracy of residual stress generation. Then, residual stress are extracted from the workpiece and analyzed in the discussion part.

2.2 Material removal rate

As the consumption of material resources increases, the material removal rate cannot be more concerned in nowadays, especially for the larger material removal volume of the complex thin wall in the machining. It can be observed from the material removal rate formula presented in Eq. 2 that the cutting depth, feed rate, tool speed, and radial width of cut are the main factors. And tool diameter does not affect the material removal rate directly, as shown in Fig. 1. If other processing parameters are the same, only half of the tool diameter is used for machining, then the material removal rate of 12 mm tool diameter (if a_e=6 mm) is two times of 6-mm tool diameter (if a_e=3 mm). Therefore, setting up and choosing the optimized process parameters are the key points to improve the material removal rate.

$$Q = Z \cdot f \cdot a_p \cdot V \cdot a_e \tag{2}$$

where Q is the material removal rate (in cubic millimeter per minute), Z is number of flutes, f is the feed rate (in millimeter per tooth), a_p is the cutting depth (in millimeter), V is the spindle speed (in revolutions per minute), and a_e is the radial width of cut (in millimeter).

2.3 Uncut chip thickness

In the previous article [26], it is concluded that residual tangential stress is influenced by the UCT. Moreover, residual radial stress, under high feed rate, is distributed with wave change, and residual radial stress under smaller feed rate is still affected by the UCT. As the UCT model built in this article (Fig. 1), two critical points (A and B) are

Table 3 Processing and tool parameters

Tool diameters (mm)	Milling path (tool)	Radial width of cut (mm)	Cutting depth (mm)	Milling speed V (rpm)	Feed rate f (mm/tooth)	Tool material (coated)	Rake angle (deg)	Clearance angle (deg)
6	Full	6	0.03~1	16,000	0.05~0.1	Carbide-grade	15	6
	Half	3						
12	Full	12						
	Half	6						

Fig. 2 Typical thin-walled part

discussed. Point A has the largest UCT in the radial width of cut, while point B has the smallest UCT. For the same feed rate, with different tool diameters, point A has the same UCT. The UCT of point B decreases as the tool diameter increases. Hence, based on established UCT model which is a function of the feed rate and tool diameter, further analysis is conducted to improve the machining precision and distribution of residual stress by optimizing the tool diameters. And it is of far-reaching significance, especially for the large area thin-walled part (Fig. 2) analyzed in this paper.

In the UCT distribution which is shown in Fig. 3, the feed rate is 0.1 and 0.2 mm/tooth, respectively. Both in Fig. 3a, b, the variations of UCT are inconsistent for different tool diameters. For the same feed rate, especially on both sides of the circular-arc areas, the maximum difference can reach three times (6 and 20 mm tool diameters compared). It means that improving the residual stress distribution is possible by controlling the UCT at these areas.

In the discussion above, for the same feed rate, the UCT can be decreased with larger tool diameters. In this paper, 6 mm (a_e=3 mm) and 12 mm (a_e=6 mm) tool diameter is selected in the milling of thin-walled part, which is presented in Fig. 4a. The UCT (6 and 12 mm tool diameter) is compared around the radial width of 3 mm.). It can be seen in Fig. 4b that the increment rate of UCT (6 mm) ranges from 1.1 to 2.05. For the same feed rate, point A of two tool diameters has the same UCT. However, the UCT of point B for 6 mm is 1.7 μm which is larger than the value 0.83 μm (12 mm). And point B has the largest difference. Therefore, the cutting forces and thermo of these two points are discussed in order to analyze the residual stress distribution and distortion in Section 4.1.

3 Experiment procedures

3.1 Machining and distortion measurement

In order to evaluate the influence of optimal selection of tool diameters on the distortion and residual stress, different processing parameters are utilized. In addition, a typical aviation thin-walled part is machined on Bridgeport machine (model XR1000, Fig. 5a), and the distortion of bottom surface is measured on Micro-Hite 3D DCC which is shown in Fig. 5b.

3.2 Measurement of machined residual stress

Generally, the measurement methods of residual stress include the drilling method (destruction), strain gage, and X-ray technology [34]. On accounting of the economics, to the machined thin-walled parts, the X-ray method can avoid to destruct the workpiece. Therefore, in this article, after the machining experiments, the high-power Canada PROTO

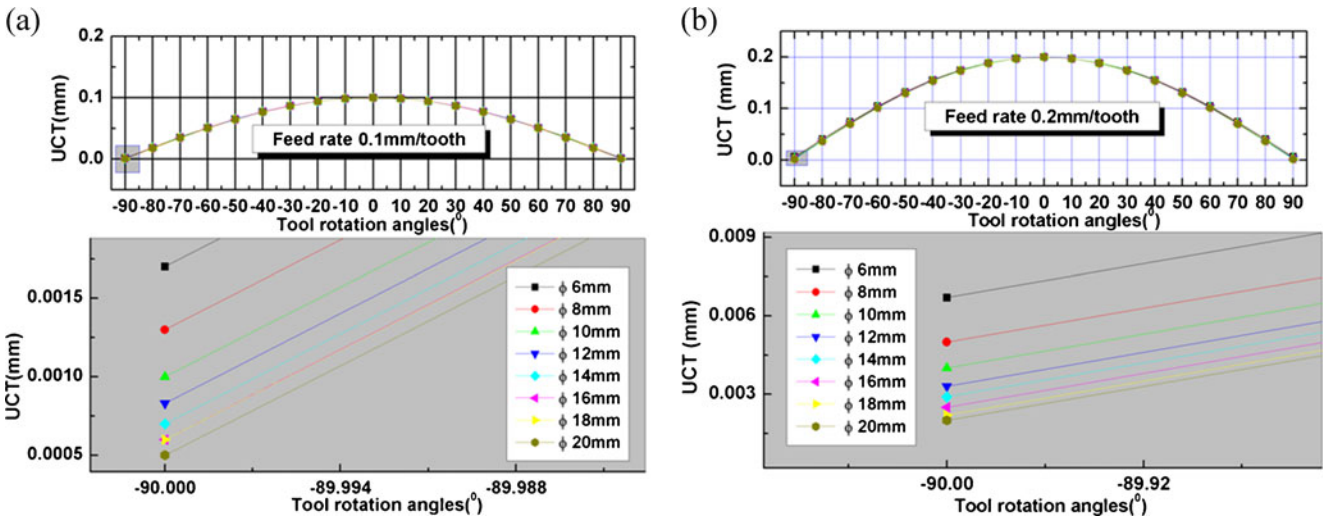

Fig. 3 Analysis of UCT under different tool diameters. **a** Feed rate 0.1 mm/tooth. **b** Feed rate 0.2 mm/tooth

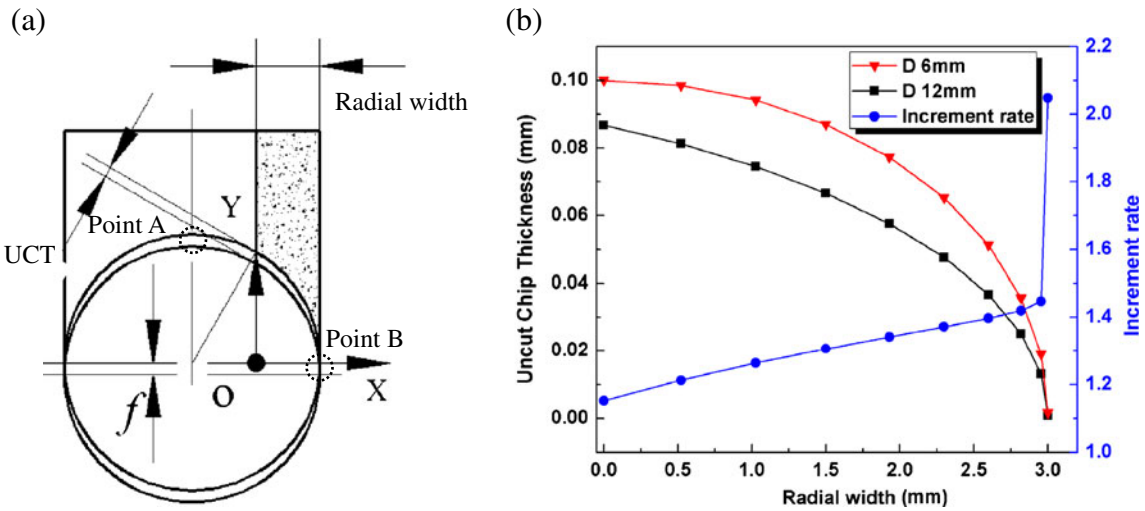

Fig. 4 **a** Analysis points. **b** Comparison of UCT

residual stress analyzer (LXRD) is utilized to measure the machined surface residual stresses according to the milling path of the thin-walled part (Fig. 6). After the machining, the part is plated on the worktable, and target points are marked. And the rotated table is used to measure the residual stress in different directions. In this paper, during the measurement, points A and B are selected as the measurement schematic shown in Fig. 6a. And the relevant parameters of stress analyzer are listed in Table 4. Generally, in the Bragg equation, it is critical to obtain elastic constant (K) [35], which is used to calculate the residual stress.

4 Results and discussions

4.1 Analysis of the cutting force and thermo influenced by different tool diameters

In the milling tool path in Fig. 6a, it can be observed that the tool radial widths of cut are composed by full and half of tool diameters. But the largest UCT of these two ways is the same (equal to feed rate); taking into account saving the computational time, only half the width of tool diameter (semi-knife) is simulated.

In general, the cutting force causes residual tensile stress. The cutting force and temperature distribution in Fig. 7a presents the friction contact among the chip, the workpiece, and the tool. There are compression force (N2) and pulled outward force (F2) in the first cutting zone around the areas of tool rake face and chip contact points. In the second cutting zone, the chip will be brought out as the tool rotates. During this process, tensile or compressive force (F1) will occur on the surface depending on the different locations. Most of the generated heat is taken away as the chip is removed, and some of them will residue in the tool. In addition, heat gradient is formed from high temperature to low temperature within the workpiece, which will cool down to generate the final distribution of residual stress after mechanical and thermal loading are released. Figure 7b

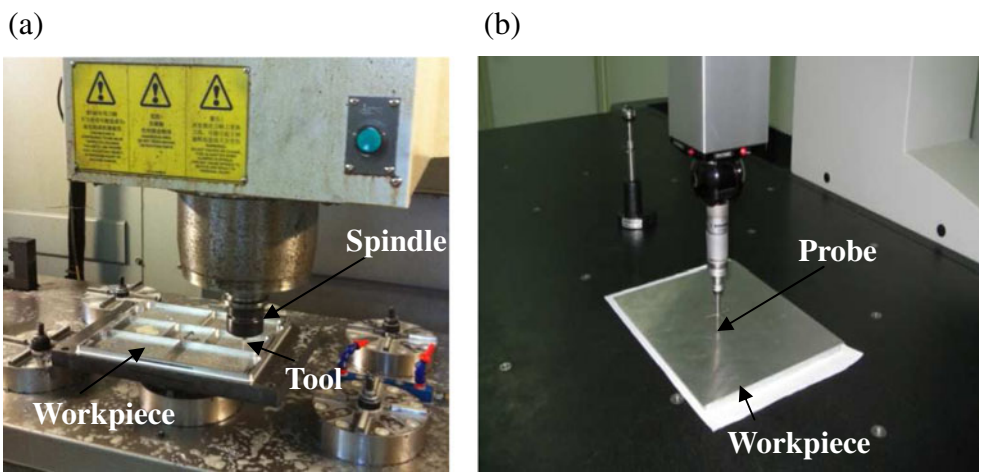

Fig. 5 **a** Machining processing. **b** Distortion measurement

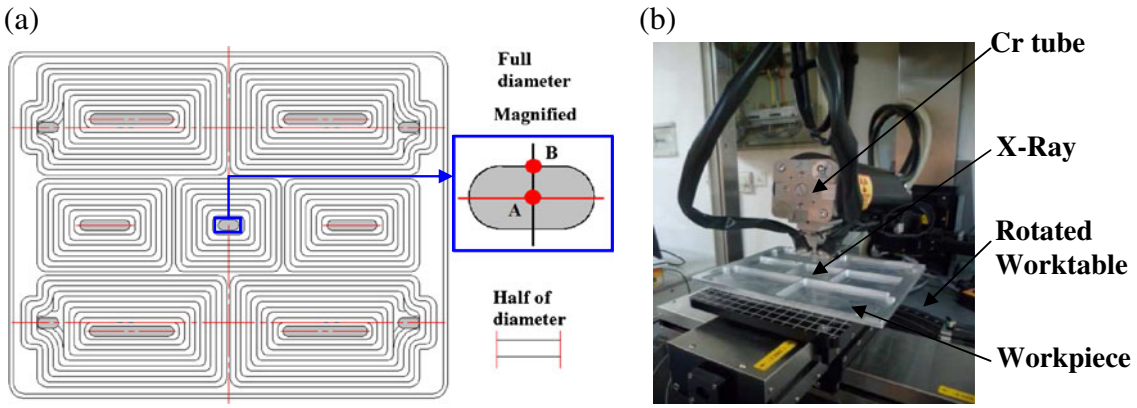

Fig. 6 **a** Milling tool path and measured points. **b** Residual stress measurement

presents the state of stress caused by the heat gradient and the cutting force. It can be seen that the third cutting zone is affected by the perpendicular cutting force (N2) and the friction force (F2) on the cutting surface. The friction force will produce burnishing effect, which generates the residual compressive stress. Throughout the milling process, the effects of the thermal stress on residual stress are determined by the stress gradient induced in the cooling process. At the beginning of the cutting, the rising of local temperature leads the part start to swell. However, the part is also restrained by the surrounding material; thus, generated thermal stress will become residual compressive stress (compressive plastic deformation). Beyond that, if plastic projective happens during this process, then residual tensile stress will generate after the part cools down to room temperature. Therefore, the thermal stress is influenced by a lot of factors such as the material properties, internal stress state, etc.

Considering that it is easy to track the value of cutting forces and temperature at different points and saving the experiment cost, in this research, AdvantEdge^{TM}-2D [29] is used. Figure 8 presents the cutting forces and temperature distribution of points A and B (at cutting speed 16,000 rpm; cutting depth 1 mm; and feed rate 0.1 mm/tooth) which are predicted by FE milling simulation; the tool diameters vary from 6 to 24 mm. For both point A and point B of the different tool diameters, it can be seen that the cutting forces (feed and vertical feed direction) decrease as the tool diameters increase. Figure 8 also describes the larger tool diameter and the higher cutting linear speed. At point A (Fig. 8a), the UCT is the same (equal to feed rate), and the cutting forces decrease (maximum by 29.6 % in X direction, by 20.7 % in Y direction) to a certain point and then balance is kept. It proves that there is limitation in decreasing forces by improving tool diameters. The maximum temperature of the chip increases as the tool diameter turns larger. However, the maximum temperature of the workpiece increases from 6 to 20 mm and then decreases as the tool diameter continues inclining (to 24 mm). At point B (Fig. 8b), the UCT decreases as the tool diameter increases; the same result can be also found in Fig. 3. The cutting forces drop significantly (maximum by 44 % in X direction, by 81.8 % in Y direction) as the tool diameter increases. Moreover, the maximum temperature of workpiece continues to decrease. The smaller cutting forces and thermo will lead to the less distortion, which is good to thin-walled part machining.

In summary, reasonable controlling of the tool diameter can improve workpiece surface temperature distribution and cutting forces. However, additional evaluation also should be considered according the shape of parts, as well as the condition of the equipments.

4.2 Analysis of the residual stress influenced by different tool diameters

In this section, as described in Section 3.2, by using X-ray stress analyzer (Fig. 6b), the residual stresses of points A and B are measured to compare the FE simulation results from AdvantEdge^{TM}-3D. The reason is

Table 4 Relevant parameters setup for residual stress measurement

Target	Aperture	Voltage	Elastic constant K (MPa/deg)	Bragg angle 2θ	Diffracting plane hkl	Numbers of beta ψ(±20°)	Oscillation beta angle
Cr	1 mm	25 kV	−98.6124	156.31°	222	11	3°

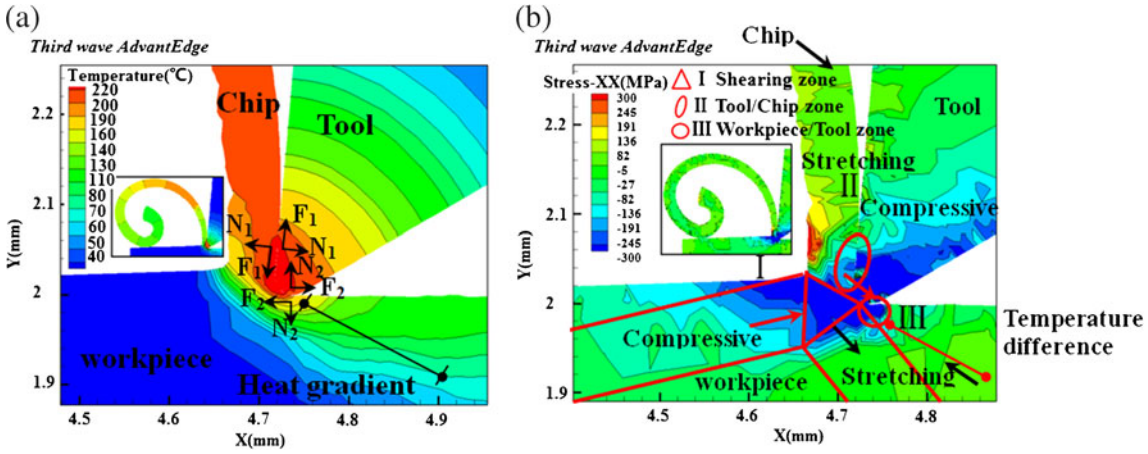

Fig. 7 **a** Analysis of cutting forces and temperature. **b** The state of stress affected by cutting force and heat gradient

that AdvantEdge^{TM}-2D cannot predict the residual stress for its lack of full part geometry (in Z direction). The following two steps present how the residual stress is extracted: (1) in the preprocessing, residual stress calculation is selected. And after the simulation is done, the inner program will calculate the residual stress. (2) According to the measurement schematic of different points (Fig. 6a), the value of each point is extracted from the software in the postprocessing. In addition, the value in depth direction can be also measured if needed. The comparisons are (magnitude of residual tangential and radial stress) presented in Fig. 9. The processing parameters and the other tool parameters are shown in Table 3. The simulation setup is the same as the experiment procedure. It can be seen that the experimental and simulation results are matched well (the maximum relative error is 13.4 % and the minimum is 4.3 %), which verify the validity of the results.

For further study, the relations among the residual stresses, UCT, and material removal rate of point A and point B under different processing parameters are shown in Table 5. The experimental and simulation model is the same as described in Section 2. It can be found in Table 5 that, for different processing parameters, the UCT of the points A and B is different, which directly lead that the residual stress distribution is also inconsistent. Generally, in the roughing process, the high material removal rate (from 76,800 to 307,200 mm^3/min) is selected, which will increase the cutting forces. As a consequence, the magnitude of residual stress will increase. For the points A and B, the residual tensile stress is formed. The higher the UCT, the larger the residual tensile stress. In the finishing processing, the material removal rate is reduced (3,840, 38,400 mm^3/min), while under high linear speed, the distribution of residual stress is improved. In addition, the residual tensile stress is generated at point A, while at point B, residual compressive stress is formed. Hence, by adjusting different processing parameters, the material removal rate can be changed accordingly. With smaller UCT and material removal rate, the

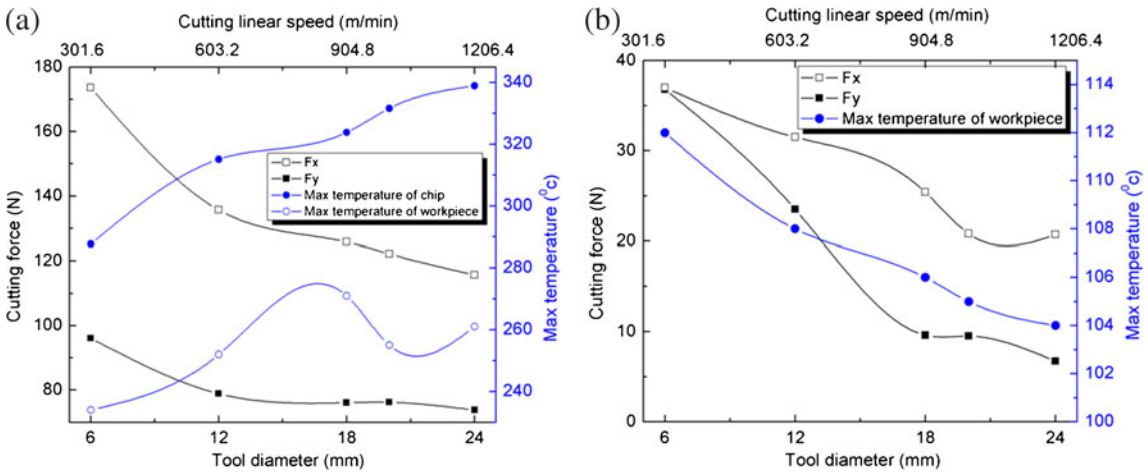

Fig. 8 Analysis of cutting forces and temperature. **a** Point A. **b** Point B

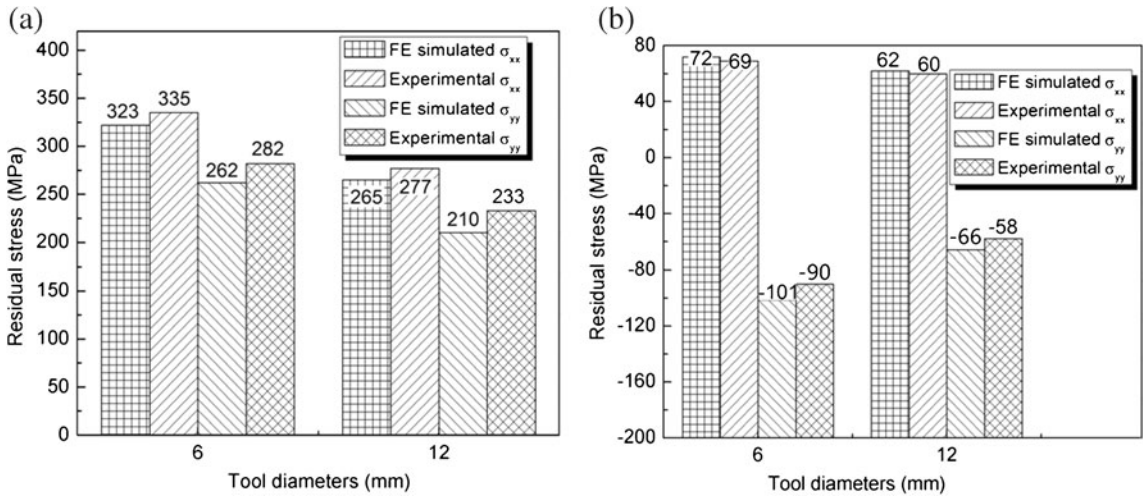

Fig. 9 Analysis of surface residual stress distribution. **a** Point A. **b** Point B

residual compressive stress will be generated around the area of point B.

Mechanical and thermal loading are the main factors which will affect the residual stress generation; in order to discuss the impact of these factors, such as the cutting forces, temperature, and residual stresses of tool diameters of 6 and 12 mm, these are listed in Table 6. It can be observed in Table 6 that when the tool diameter increases to 12 mm, the residual tangential stress and radial stress at point A are reduced by 17.3 and 17.3 %, respectively, while the tangential force and normal force are reduced by 21.8 and 17.9 %, respectively. The temperature is increased by 8.7 %. Hence, the influence of heat gradient on residual tangential stress is more significant than residual radial stress. At point B, larger tool diameter, the tangential force (by 36.1 %) and normal force (by 14.8 %) decrease, as well as the temperature of workpiece surface declines by

Table 5 Analysis of residual stress and UCT under different processing parameters

Point	Processing parameters			Linear speed (m/min)	UCT (mm)	Material removal rate (mm^3/min)	Residual tangential stress (MPa)		Residual radial stress (MPa)	
	Milling speed (rev/min)	Feed rate (mm/t)	Cutting depth (mm)				FE	EXP	FE	EXP
A	8,000	0.2	2	301.6	0.2	153,600	280	296	110	107
B	8,000	0.2	2	301.6	0.0033		121	110	356	372
A	12,000	0.2	2	452.4	0.2	230,400	421	444	257	289
B	12,000	0.2	2	452.4	0.0033		165	176	112	123
A	16,000	0.2	2	603.2	0.2	307,200	376	389	205	216
B	16,000	0.2	2	603.2	0.0033		160	171	130	125
A	16,000	0.05	2	603.2	0.05	76,800	390	409	225	241
B	16,000	0.05	2	603.2	0.0002		42	32	−80	−88
A	10,000	0.1	0.8	377.0	0.1	38,400	300	320	152	165
B	10,000	0.1	0.8	377.0	0.00083		−40	−28	−41	−35
A	16,000	0.05	1	603.2	0.05	38,400	310	333	280	290
B	16,000	0.05	1	603.2	0.0002		−110	−122	−99	−125
A	8,000	0.1	1	301.6	0.1	38,400	367	388	183	189
B	8,000	0.1	1	301.6	0.00083		−42	−38	−29	−43
A	16,000	0.1	0.5	603.2	0.1	38,400	265	280	129	141
B	16,000	0.1	0.5	603.2	0.00083		−29	−27	−38	−54
A	16,000	0.05	0.1	603.2	0.05	3,840	45	51	65	72
B	16,000	0.05	0.1	603.2	0.0002		−21	−25	−31	−33

Table 6 Analysis of cutting forces, temperature, and residual stress

Tool diameter	Point	Cutting forces F(N)				Temperature T(°C)		Residual stress σ (Mpa)			
		Tangential force (X)		Normal force (Y)		Temperature of workpiece		Tangential		Radial	
6	A	173.6	↓21.8 %	83.1	↓17.9 %	234	↑8.7 %	335	↓17.3 %	282	↓17.3 %
12		135.4		69.4		252		277		233	
6	B	37	↓14.8 %	36.8	↓36.1 %	112	↓3.6 %	69	↓13%	−90	↓35.6 %
12		31.5		23.5		108		60		−58	

3.6 %. However, the residual tangential stress and radial stress decrease by 35.6 and 13 %, respectively. The same conclusions can be summarized that residual radial stress has less influence from heat gradient. Consequently, residual tangential stress is determined by the cutting force and heat gradient, while residual radial stress is mainly generated by the cutting force.

In order to further analyze the subsurface residual stress distribution in the depth direction by extracting the results of points A and B from FE simulation, the comparisons of residual stress in two directions are presented in Fig. 10. The cutting speed is 16,000 rpm, the cutting depth is 1 mm, and the feed rate is 0.1 mm/tooth; other parameters are the same as in Table 3. At point A, for the residual tangential (σ_{xx}) and radial stress (σ_{yy}) beneath the surface, the maximum residual compressive stress is smaller for 12 mm tool diameter. Furthermore, the depth of the position is deeper than 6-mm tool diameter. At point B, the tool diameter is increased to 12 mm, and the maximum residual tangential stress and radial stress are decreased by 65.4 and 15.2 %, respectively. In addition, the distribution of residual stress beneath the surface is more uniform than using 6 mm tool diameter. All these results are good to the final shape of products. Hence, by increasing the tool diameter, the deeper and uniform distribution of the residual stress will be generated, and the smaller value will be achieved, which are good to maintain the stability of thin-walled parts after processing.

4.3 Comparisons of machined distortion influenced by different tool diameters

In the previous Section 4.1, the distributions of cutting forces and temperature under different tool diameters are discussed. In this section, plastic deformation of the workpiece is compared to analyze its influence on the machined surface with different tool diameters (range from 6 to 20 mm, at cutting speed 160,00 rpm, cutting depth 2 mm, and feed rate 0.1 mm/tooth).

Plastic deformation is measured and described in Fig. 11. As tool diameter increases to 20 mm, the maximum deformation on the surface is different. It can be found that when the tool diameter is 6 mm, the maximum deformation value is 16 μm, while increasing the tool diameter to 12 mm, the maximum deformation value can be reduced to 5.8 μm (by 63.8 %). With further increase in the tool diameter, the maximum deformation still keeps a downward trend. This is because for large tool diameter, the cutting forces will decline corresponding, as the results discussed in Section 4.1.

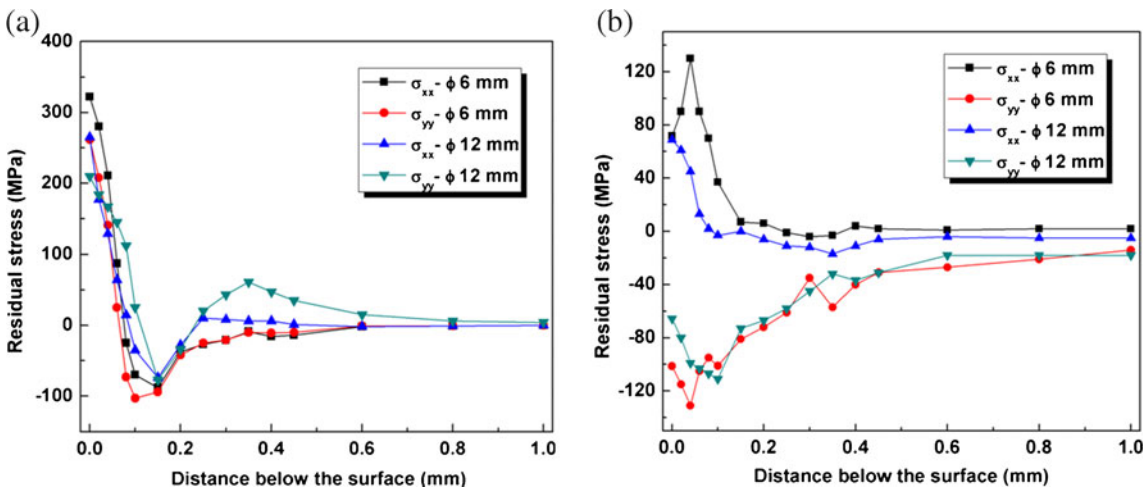

Fig. 10 Analysis of subsurface residual stress distribution. **a** Point A. **b** Point B

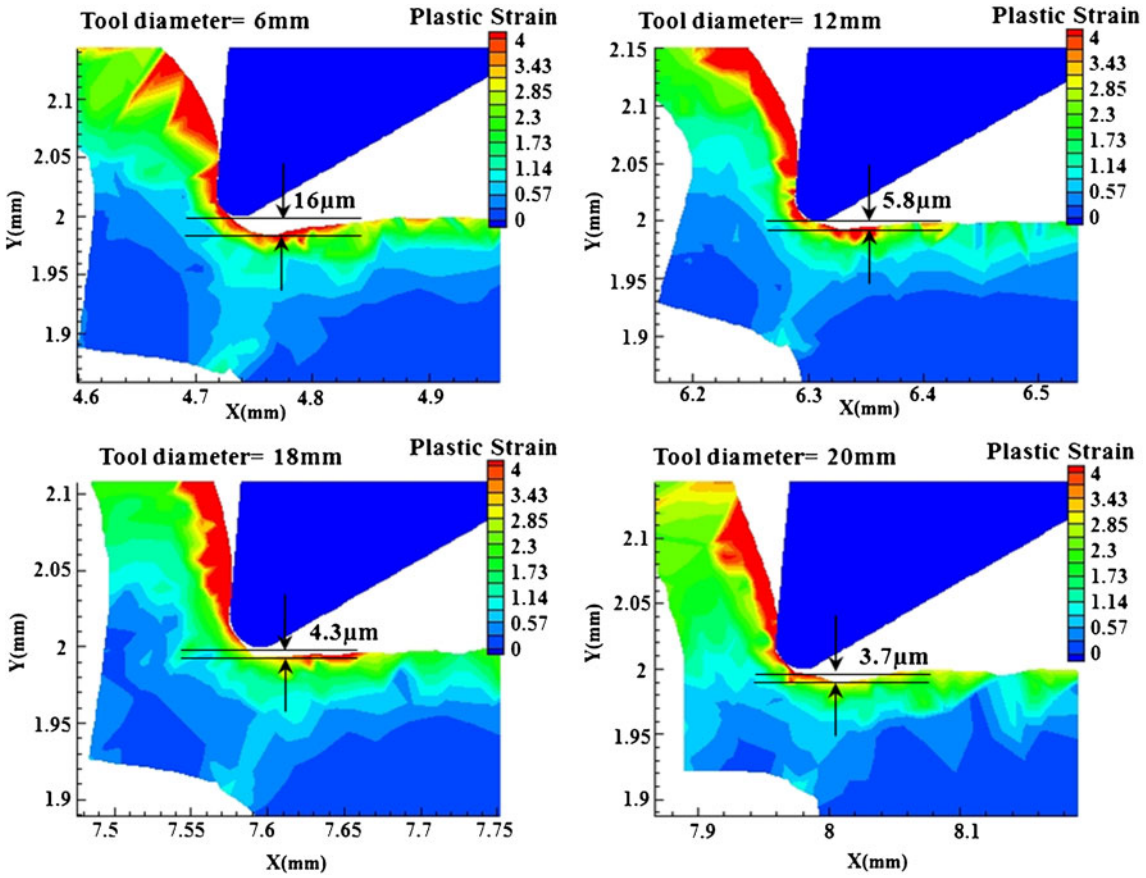

Fig. 11 Analysis of the plastic deformation under different tool diameters

According to the methods analyzed in this article, different tool diameters (6 and 12 mm) are selected to machining the thin-walled part (Fig. 2), and the other processing parameters are the same. Because the specific machining processing parameters of parts are confidential, only the final distortion results will be given. The deformation contour by fitting the distortion measured after the experiments are finished is presented in Fig. 12. The maximum distortion of thin-walled workpiece using 6 mm tool diameter is 446.3 μm (Fig. 12a); however, the maximum distortion using 12 mm tool diameter is 171 μm (Fig. 12b), and the overall deformation drops by 61.7 %. The result is also getting close to the FE analysis of plastic deformation which is 63.8 %, proving that the method is effective.

5 Conclusions

For thin-walled part machining, many factors are concerned such as the processing parameters of the products, fixtures, machines, and other factors; however, it is still difficult to control the distortion and residual stress. Therefore, how to

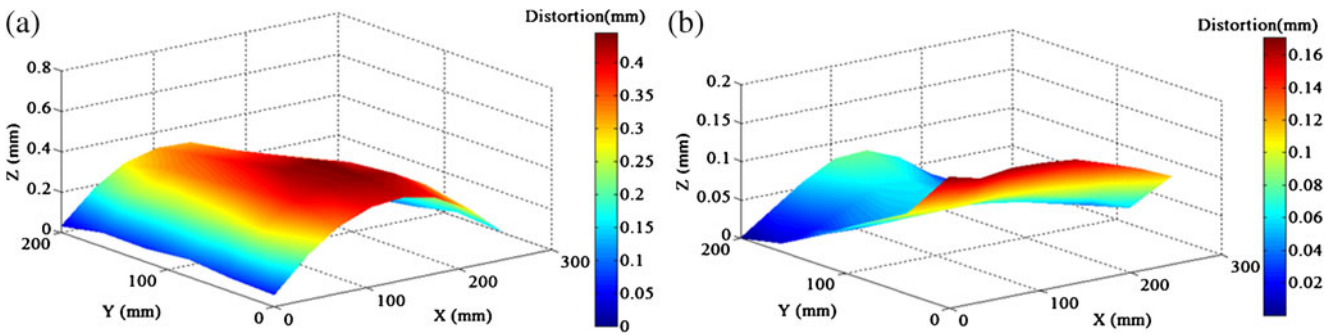

Fig. 12 Distortion comparison of bottom surface. **a** 6 mm. **b** 12 mm

improve and optimize these factors are always discussed and analyzed by the researchers. In this paper, under high-speed milling, different diameter tools are utilized, and then the cutting force, heat generation, distortion and residual stresses are analyzed. In addition, a thin-walled part is machined to evaluate the machining precision.

In the findings, large tool diameter will directly reduce the UCT, and the value is also inconsistent in different locations around the radial width of cut. Two points A and B are selected to discuss that the cutting forces decrease as the tool diameter increases. Furthermore, residual stress distribution turns to more uniform with larger tool diameter. And residual tangential stress is determined by the cutting force and heat gradient, while residual radial stress is mainly generated by the cutting force. Moreover, the material removal rate improved accordingly with 12 mm diameter tool. In addition, the typical thin-walled part is machined, and the maximum distortion of the workpiece is deduced from 446.3 to 171 μm by utilizing 12 mm tool diameter, which can be well matched with the plastic deformation found in the FE simulation. Hence, in the thin-walled part machining, choosing reasonable tool diameter is pretty important and effective, and this method can provide a reference and technical support to control the machining accuracy and residual stress. As a future work for thin-walled part machining, optimization of tool path is to be conducted, and also the appropriate processing parameters will be combined and optimized.

Acknowledgments The authors want to thank for the support from the National Natural Science Foundation (no. 50975046) and Shanghai Leading Academic Discipline Project (no. B602). We also appreciate the help from Shanghai MaiXun Machine Tool Technology Co. Ltd. for machining experiments. The author Mr. Jiang also thanks the support from Donghua University Innovation Funding of PHD thesis (11D10313).

References

1. Li JL, Jing LL, Chen M (2009) An FEM study on residual stresses induced by high-speed end-milling of hardened steel SKD11. J Mater Process Technol 209:4515–4520
2. Guo YB, Barkey ME (2004) FE-simulation of the effects of machining-induced residual stress profile on rolling contact of hard machined components. Int J Mech Sci 46:371–388
3. Zong WJ, Li D, Cheng K, Sun T, Liang YC (2007) Finite element optimization of diamond tool geometry and cutting-process parameters based on surface residual stresses. Int J Adv Manuf Technol 32:666–674
4. Özel T, Zeren E (2007) Finite element modeling the influence of edge roundness on the stress and temperature fields induced by high-speed machining. Int J Adv Manuf Technol 35:255–267
5. El-Axir MH (2002) A method of modeling residual stress distribution in turning for different materials. Int J Mach Tools Manuf 42:1055–1063
6. Ulutan D, Alaca BE, Lazoglu I (2007) Analytical modeling of residual stresses in machining. J Mater Process Technol 183:77–87
7. Lazoglu I, Ulutan D, Alaca BE, Engin S, Kaftanoglu B (2008) An enhanced analytical model for residual stress prediction in machining. CIRP Annals - Manuf Technol 57:81–84
8. Liang SY, Su JC (2007) Residual stress modeling in orthogonal machining. CIRP Annals—Manuf Technol 56(1):65–68
9. Ficquet X, Truman CE, Kingston E, Smith DJ (2006) Measurement of residual stresses in aluminium alloy aerospace components. 25th International Congress of the Aeronautical Sciences
10. Caruso S, Umbrello D, Outeiro JC, Filice L, Micari F (2011) An experimental investigation of residual stresses in hard machining of AISI 52100 steel. Pro Eng 19:67–72
11. Rossini NS, Dassisti M, Benyounis KY, Olabi AG (2012) Methods of measuring residual stresses in components. Mater Des 35:572–588
12. Borja C, Virginia GN, Oscar G, Ana A, Carmen S (2011) Influences of turning parameters in surface residual stresses in AISI 4340 steel. Int J Adv Manuf Technol 53:911–919
13. Jacobus K, DeVor RE, Kapoor SG (2000) Machining-induced residual stress: experimentation and modeling. J Manuf Sci Eng 122(1):20–30
14. Wei Y, Wang XW (2007) Computer simulation and experimental study of machining deflection due to original residual stress of aerospace thin-walled parts. Int J Adv Manuf Technol 33:260–265
15. Outeiroa JC, Umbrello D, Saoubi RM (2006) Experimental and numerical modelling of the residual stresses induced in orthogonal cutting of AISI 316L steel. Int J Mach Tools Manuf 46:1786–1794
16. Kuang HF, Wu CF (1995) A residual stress model for the milling of aluminum alloy(2014-T6). J Mater Process Technol 51:87–105
17. Mohammadpour M, Razfar MR, Jalili Saffar R (2010) Numerical investigating the effect of machining parameters on residual stresses in orthogonal cutting. Simul Model Pract Th 18:378–389
18. Fan N, Chen M, Guo PQ, (2009) Simulation of cutting tool geometry parameters impact on residual stress. 2009 Chinese Control and Decision Conference (CCDC 2009): 5472–5475.
19. Mohamed NA, Ng EG, Elbestawi MA (2007) Modelling the effects of tool-edge radius on residual stresses when orthogonal cutting AISI 316L. Int J Mach Tools Manuf 47(2):401–411
20. Tang ZT, Liu ZQ, Pan YZ, Wan Y, Ai X (2009) The influence of tool flank wear on residual stresses induced by milling aluminum alloy. J Mater Process Technol 209(2):4502–4508
21. Lin ZC, Lai WL, Lin HY, Liu CR (1997) Residual stresses with different tool flank wear lengths in the ultra-precision machining of Ni-P alloys. J Mater Process Technol 65:116–126
22. Muñoz-Sánchez A, Canteli JA, Cantero JL, Miguélez MH (2011) Numerical analysis of the tool wear effect in the machining induced residual stresses. Simul Model Pract Th 19:872–886
23. Robinson JS, Tanner DA, Truman CE, Paradowska AM, Wimpory RC (2012) The influence of quench sensitivity on residual stresses in the aluminium alloys 7010 and 7075. Mater Charact 65:73–85
24. Richter-Trummer V, Suzano E, Beltrão M, Roos A, dos Santos JF, de Castro PMST (2012) Influence of the FSW clamping force on the final distortion and residual stress field. Mater Sci Eng, A 538:81–88
25. Li BZ, Jiang XH, Jing HJ, Zuo XY (2011) High-speed milling characteristics and the residual stresses control methods analysis of thin-walled parts. Adv Mater Res 223:456–463
26. Jiang XH, Li BZ, Yang JG, Zuo XY, Li K (2012) An approach for analyzing and controlling residual stress generation during high-speed circular milling. Int J Adv Manuf Technol. doi:10.1007/s00170-012-4421-8, Online First™
27. Kuruppu MD, Williams JF, Bridgford N, Jones R, Stouffer DC (1992) Constitutive modelling of the elastic–plastic behaviour of 7050-T7451 aluminium alloy. J Strain Anal Eng Des 27:85–92

28. Third Wave Systems, Inc. (2010) AdvantEdge v5.6-014 machining simulation software. Minneapolis, MN
29. Hu HJ, Huang WJ (2012) Effects of turning speed on high-speed turning by ultrafine-grained ceramic tool based on 3D finite element method and experiments. Int J Adv Manuf Technol. doi:10.1007/s00170-012-4535-z
30. Jing S, Liu CR (2004) The influence of material models on finite element simulation of machining. J Manuf Sci Eng 126:849–857
31. Jiang F, Li JF, Sun J, Zhang S, Wang ZQ, Yan L (2010) Al7050-T7451 turning simulation based on the modified power-law material model. Int J Adv Manuf Technol 48:871–880
32. Marusich TD, Ortiz M (1995) Modelling and simulation of high-speed machining. J Num Meth Eng 38(21):3675–3694
33. Marusich TD, Askari E (2001) Modeling residual stress and workpiece quality in machined surfaces. Third Wave Systems Inc, Minneapolis
34. Coto B, Navas VG, Gonzalo O, Aranzabe A, Sanz C (2011) Influences of turning parameters in surface residual stresses in AISI 4340 steel. Int J Adv Manuf Technol 53:911–919
35. Eigenmann B, Macherauch E (1996) Roentgenographische untersuchung von spannugszustaenden in werkstoffen (teil 3) Mat-wiss U Werkstoff technik 27: 427–431